arXiv:2002.00411v2 [cond-mat.stat-mech] 19 Feb 2020

Finite-size scaling of typicality-based estimates

Jürgen Schnack,[1,*] Johannes Richter,[2,3,†] Tjark Heitmann,[4] Jonas Richter,[4] and Robin Steinigeweg[4,‡]

[1] *Fakultät für Physik, Universität Bielefeld, Postfach 100131, D-33501 Bielefeld, Germany*
[2] *Institut für Theoretische Physik, Universität Magdeburg, P.O. Box 4120, D-39016 Magdeburg, Germany*
[3] *Max-Planck-Institut für Physik Komplexer Systeme, Nöthnitzer Straße 38, 01187 Dresden, Germany*
[4] *Fachbereich Physik, Universität Osnabrück, Barbarastr. 7, D-49076 Osnabrück, Germany*

(Dated: August 15, 2021)

According to the concept of typicality, an ensemble average can be accurately approximated by an expectation value with respect to a single pure state drawn at random from a high-dimensional Hilbert space. This random-vector approximation, or trace estimator, provides a powerful approach to, e.g., thermodynamic quantities for systems with large Hilbert-space sizes, which usually cannot be treated exactly, analytically or numerically. Here, we discuss the finite-size scaling of the accuracy of such trace estimators from two perspectives. First, we study the full probability distribution of random-vector expectation values and, second, the full temperature dependence of the standard deviation. With the help of numerical examples, we find pronounced Gaussian probability distributions and the expected decrease of the standard deviation with system size, at least above certain system-specific temperatures. Below and in particular for temperatures smaller than the excitation gap, simple rules are not available.

I. INTRODUCTION

Methods such as the finite-temperature Lanczos method (FTLM) [1–7], that rest on trace estimators [1, 8–16] and thus – in more modern phrases – on the idea of typicality [17–20], approximate equilibrium thermodynamic observables with very high accuracy [2, 21]. In the canonical ensemble, the observable can be evaluated either with respect to a single random vector $|\,r\,\rangle$,

$$O^{\mathrm{r}}(T) \approx \frac{\langle\, r \,|\, \underset{\sim}{O} e^{-\beta \underset{\sim}{H}} \,|\, r \,\rangle}{\langle\, r \,|\, e^{-\beta \underset{\sim}{H}} \,|\, r \,\rangle} \,, \tag{1}$$

or with respect to an average over R random vectors,

$$O^{\mathrm{FTLM}}(T) \approx \frac{\sum_{r=1}^{R} \langle\, r \,|\, \underset{\sim}{O} e^{-\beta \underset{\sim}{H}} \,|\, r \,\rangle}{\sum_{r=1}^{R} \langle\, r \,|\, e^{-\beta \underset{\sim}{H}} \,|\, r \,\rangle} \,, \tag{2}$$

where numerator and denominator are averaged with respect to the same set of random vectors. The components of $|\,r\,\rangle$ with respect to an orthonormal basis are taken from a Gaussian distribution with zero mean (Haar measure [22–24]), but in practice other distributions work as well. T, β, and $\underset{\sim}{H}$ denote the temperature, inverse temperature and the Hamiltonian, respectively.

In this work, we discuss the accuracy of Eqs. (1) and (2), where we particularly focus on the dependence of this accuracy on the system size or, to be more precise, the dimension of the effective Hilbert space spanned by thermally occupied energy eigenstates. While it is well established that the accuracy of both equations increases with the square root of this dimension, we shed light on the size dependence from two less studied perspectives. First, we study the full probability distribution of random-vector expectation values, for the specific example of magnetic susceptibility and heat capacity in quantum spin systems on a one-dimensional lattice. At high temperatures, our numerical simulations unveil that these distributions are remarkably well described by simple Gaussian functions over several orders of magnitudes. Moreover, they clearly narrow with the inverse square root of the Hilbert-space dimension towards a δ function. Decreasing temperature at fixed system size, we find the development of broader and asymmetric distributions. Increasing the system size at fixed temperature, however, distributions become narrow and symmetric again. Thus, the mere knowledge of the standard deviation turns out to be sufficient to describe the full statistics of random-vector expectation values – at least at not too low temperatures.

The second central perspective of our work is taken by performing a systematic analysis of the scaling of the standard deviation with the system size, over the entire range of temperature and in various quantum spin models including spin-1/2 and spin-1 Heisenberg chains, critical spin-1/2 sawtooth chains, as well as cuboctahedra with spins 3/2, 2, and 5/2. We show a monotonous decrease of the standard deviation with increasing effective Hilbert-space dimension, as long as temperature is high compared to some system-specific low-energy scale. Below this scale, the scaling can become unsystematic if only a very few low-lying energy eigenstates contribute. However, when averaging according to Eq. (2) over a decent number (~ 100) of random vectors, one can still determine the thermodynamic average very accurately in all examples considered by us. A quite interesting example constitutes the critical spin-1/2 sawtooth chain, where a single state drawn at random is enough to obtain this average down to very low temperatures.

This paper is organized as follows. In Sec. II we briefly

* jschnack@uni-bielefeld.de
† Johannes.Richter@physik.uni-magdeburg.de
‡ rsteinig@uos.de

recapitulate models, methods, as well as typicality-based estimators. In Sec. III we present our numerical examples both for frustrated and unfrustrated spin systems. The paper finally closes with a summary and discussion in Sec. IV.

II. METHOD

In this article we study several spin systems at zero magnetic field. They are of finite size and described by the Heisenberg model,

$$\underset{\sim}{H} = \sum_{i<j} J_{ij}\, \vec{\underset{\sim}{s}}_i \cdot \vec{\underset{\sim}{s}}_j \ , \tag{3}$$

where the sum runs over ordered pairs of spins. Here and in the following operators are marked by a tilde, i.e. $\vec{\underset{\sim}{s}}_i$ denotes the spin-vector operator at site i. J_{ij} denotes the exchange interaction between a spin at site i and a spin at site j. With the sign convention in (3), $J_{ij} > 0$ corresponds to antiferromagnetic interaction.

Numerator and denominator of (2), the latter is the partition function, are evaluated using a Krylov-space expansion, i.e. a spectral representation of the exponential in a Krylov space with $|\, r\,\rangle$ as starting vector of the Krylov-space generation, compare [1, 4]. One could equally well employ Chebyshev polynomials [13, 25, 26] or integrate the imaginary-time Schrödinger equation with a Runge-Kutta method [27–29], the latter is used later in this paper as well.

If the Hamiltonian $\underset{\sim}{H}$ possesses symmetries, they can be used to block-structure the Hamiltonian matrix according to the irreducible representations of the employed symmetry groups [4, 5], which yields for the partition function

$$Z^{\mathrm{FTLM}}(T) \approx \sum_{\gamma=1}^{\Gamma} \frac{\dim[\mathcal{H}(\gamma)]}{R} \times \sum_{r=1}^{R} \sum_{n=1}^{N_L} e^{-\beta\epsilon_n^{(r)}} |\langle\, n(r)\,|\, r\,\rangle|^2 \ . \tag{4}$$

$\mathcal{H}(\gamma)$ labels the subspace that belongs to the irreducible representation γ, N_L denotes the dimension of the Krylov space, and $|\, n(r)\,\rangle$ is the n-th eigenvector of $\underset{\sim}{H}$ in this Krylov space grown from $|\, r\,\rangle$. The energy eigenvalue is $\epsilon_n^{(r)}$. To perform the Lanczos diagonalization for larger system sizes, we use the public code *spinpack* [30, 31].

In our numerical studies we evaluate the uncertainty of a physical quantity by repeating its numerical evaluation N_S times. For this statistical sample we define the standard deviation of the observable in the following way:

$$\delta(O) = \sqrt{\frac{1}{N_S}\sum_{r=1}^{N_S}\left[O^{\mathrm{m}}(T)\right]^2 - \left[\frac{1}{N_S}\sum_{r=1}^{N_S} O^{\mathrm{m}}(T)\right]^2} = \sqrt{\overline{\left[O^{\mathrm{m}}(T)\right]^2} - \left[\overline{O^{\mathrm{m}}(T)}\right]^2} \ . \tag{5}$$

$O^{\mathrm{m}}(T)$ is either evaluated according to Eq. (1) (m=r) or to Eq. (2) (m=FTLM), depending on whether the fluctuations of approximations with respect to one random vector or with respect to an average over R vectors shall be investigated.

We consider two physical quantities, the zero-field susceptibility as well as the heat capacity. Both are evaluated as variances of magnetization and energy, respectively, i.e.

$$\chi(T) = \frac{(g\mu_B)^2}{k_B T}\left[\left\langle (\underset{\sim}{S}^z)^2\right\rangle - \left\langle \underset{\sim}{S}^z\right\rangle^2\right], \tag{6}$$

$$C(T) = \frac{k_B}{(k_B T)^2}\left[\left\langle \underset{\sim}{H}^2\right\rangle - \left\langle \underset{\sim}{H}\right\rangle^2\right] . \tag{7}$$

We compare our results with the well-established high-temperature estimate

$$\delta\langle \underset{\sim}{Q}\rangle \simeq \langle \underset{\sim}{Q}\rangle \frac{\alpha}{\sqrt{Z_{\mathrm{eff}}}} \ , \qquad Z_{\mathrm{eff}} = \mathrm{tr}\left[e^{-\beta(\underset{\sim}{H}-E_0)}\right] \ . \tag{8}$$

Here E_0 denotes the ground-state energy. In general the prefactor α depends on the specific system, its structure and size, as well as on temperature [18, 19], but empirically often turns out to be a constant of order $\alpha \approx 1$ for high enough temperatures, compare [2, 6, 21]. Rigorous error bounds, see Refs. [19, 32], share the dependence on $1/\sqrt{Z_{\mathrm{eff}}}$, but lead to a prefactor that can be substantially larger than the empirical finding.

III. NUMERICAL RESULTS

We now present our numerical results. First, in the following Sec. III A, the full probability distribution of random-vector expectation values is discussed for shorter spin chains, where this distribution can be easily obtained by generating a large set of different random vectors. In the remainder of Sec. III the size dependence of the standard deviation is investigated for longer spin chains of spin $s = 1/2$ and $s = 1$, respectively, which are treated by Lanczos methods. The interesting behavior of a quantum critical delta chain is studied as well. Finally, we discuss the dependence of the standard deviation on the spin quantum number for a body of fixed size, the cuboctahedron.

A. Distribution of random-vector expectation values for smaller antiferromagnetic spin-1/2 chains

As a first step, in order to judge the accuracy of the single-state estimate in Eq. (1), it is instructive to study its full probability distribution p, obtained by drawing many [here $\mathcal{O}(10^4 - 10^6)$] random vectors. To be more precise, we evaluate the numerator of Eq. (1) for different random states $|\,r\,\rangle$, while its denominator is calculated as the average over all $|\,r\,\rangle$,

$$\frac{\langle\, r\,|\, \underset{\sim}{O} e^{-\beta \underset{\sim}{H}}\,|\, r\,\rangle}{\sum_{r=1}^{R} \langle\, r\,|\, e^{-\beta \underset{\sim}{H}}\,|\, r\,\rangle} \,. \tag{9}$$

The advantage of using this equation, instead of Eq. (1), is that the mean coincides with Eq. (2), the latter should be used to correctly obtain the low-temperature average in system of finite size [21]. However, at sufficiently high temperatures or in sufficiently large systems, one might equally well use Eq. (1), as we have checked.

The single results for Eq. (9) are then collected into bins of appropriate width in order to form a "smooth" distribution p. While one might expect that p will be approximately symmetric around the respective thermodynamic average, the width of the distribution indicates how reliable a single random vector can approximate the ensemble average.

In this Section, we study the probability distribution p (in the following denoted as p_χ and p_C) for the quantities $\chi(T)T/N$ and $C(T)T^2/N$, and exemplarily consider the one-dimensional spin-1/2 Heisenberg model with antiferromagnetic nearest-neighbor coupling $J > 0$ and chain length N. Note that, as discussed in the upcoming Secs. III B - III E, details of the model can indeed have an impact on the behavior of p in certain temperature regimes. Note further, that we focus in this Section on small to intermediate system sizes $N \leq 20$, where p can be easily obtained by generating a large set of different random vectors and evolving these vectors in imaginary time by, e.g., a simple Runge-Kutta scheme. We have checked that the Runge-Kutta scheme employed in this Section has practically no impact on p.

To begin with, in Fig. 1 (a), p_χ is shown for different chain lengths $N = 12, \ldots, 20$ at infinite temperature $\beta J = 0$. For all values of N shown here, we find that p_χ is well described by a Gaussian distribution [33] over several orders of magnitude. While the mean of these Gaussians is found to accurately coincide with the thermodynamic average $\lim_{T\to\infty} \chi(T)T/N = 1/4$ [34], we moreover observe that the width of the Gaussians becomes significantly narrower upon increasing N. This fact already visualizes that the accuracy of the estimate in Eq. (1) improves for increasing Hilbert-space dimension. In particular, as shown in the inset of Fig. 1, the standard deviation $\delta(\chi)$ scales as $\delta(\chi) \propto 1/\sqrt{d}$, where $d = 2^N$ is the dimension of the Hilbert space. This is in agreement with Eq. (8) for $\alpha \approx 1.2$ and $Z_{\text{eff}} = d$ at $\beta = 0$. Note that since p_χ is found to be a Gaussian, the width $\delta(\chi)$ is sufficient to describe the whole distribution (apart from the average).

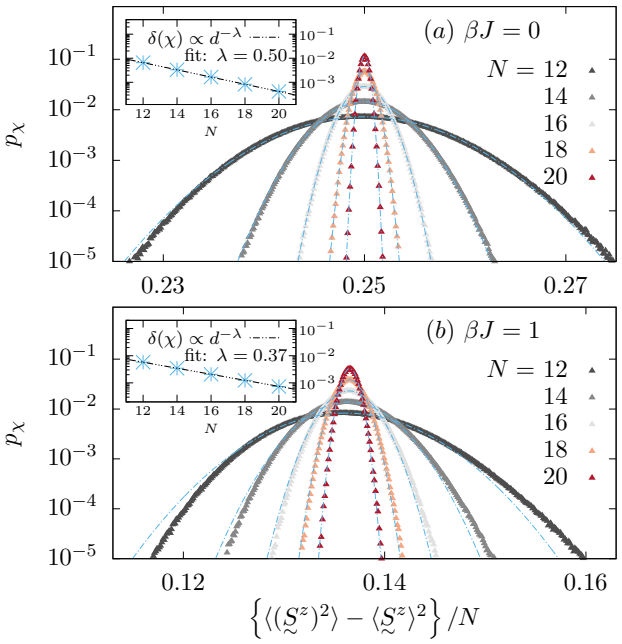


Figure 1. (a) Probability distribution of the susceptibility $\chi(T)T/N$ evaluated from independently drawn single states according to Eq. (9). Data is shown for different system sizes $N = 12, \ldots, 20$ at infinite temperature $\beta J = 0$. The dashed lines indicate Gaussian fits to the data. The inset shows the standard deviation $\delta(\chi)$ versus N, which scales as $\delta(\chi) \propto 1/\sqrt{d}$ with Hilbert-space dimension $d = 2^N$. (b) Same data as in (a) but now for the finite temperature $\beta J = 1$.

To proceed, Fig. 1 (b) again shows the probability distribution p_χ, but now for the finite temperature $\beta J = 1$. There are two important observations compared to the previous case of $\beta J = 0$. First, for small $N = 12$, one clearly finds that p_χ now takes on an asymmetric shape and the tails are not described by a Gaussian anymore. Importantly, however, upon increasing the system size N, p_χ becomes narrower and eventually turns into a Gaussian again. One may speculate about possible reasons for the observed asymmetry: It might reflect an asymmetry of the distribution, which is already present at $\beta = 0$ and small N, and then increases with increasing β; or it might also stem from the boundedness (positivity) of the observables, although the bounds are still far away for the presented case of $\beta J = 1$ in Fig. 1 (b). While this asymmetry remains to be explored in more detail in future work, it is expected that the Gaussian shape breaks down in small dimensions of the effective Hilbert space dimensions [33]. It is worth pointing out that, even for very large dimensions, the very outer tails of the distribution are expected to be of non-Gaussian nature [33]. Yet, these tails are hard to resolve in our numerical simulations, since a huge number of samples would be needed.

As a second difference compared to $\beta J = 0$, we find

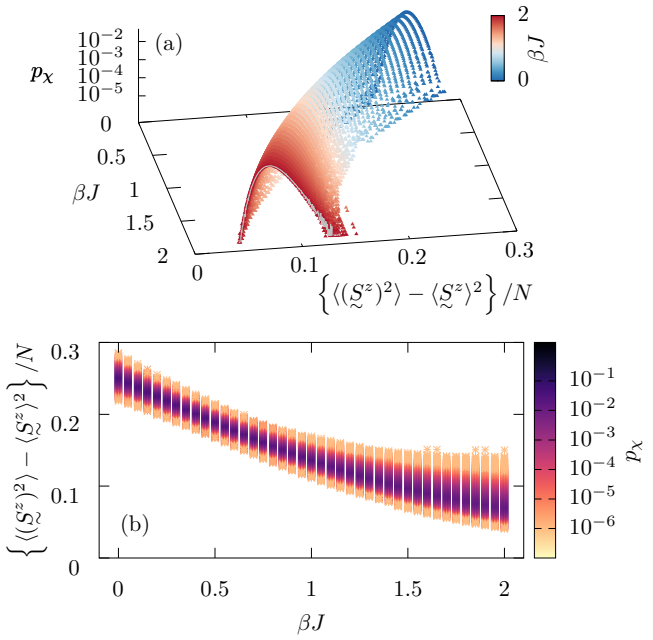


Figure 2. (a) Probability distribution of the susceptibility $\chi(T)T/N$ for various temperatures $0 \leq \beta J \leq 2$ at the fixed system size $N = 12$ obtained by ED (symbols). For comparison, data obtained by Runge-Kutta at $\beta J = 2$ is shown as well (curve). (b) Same data as in (a), but now as a contour plot.

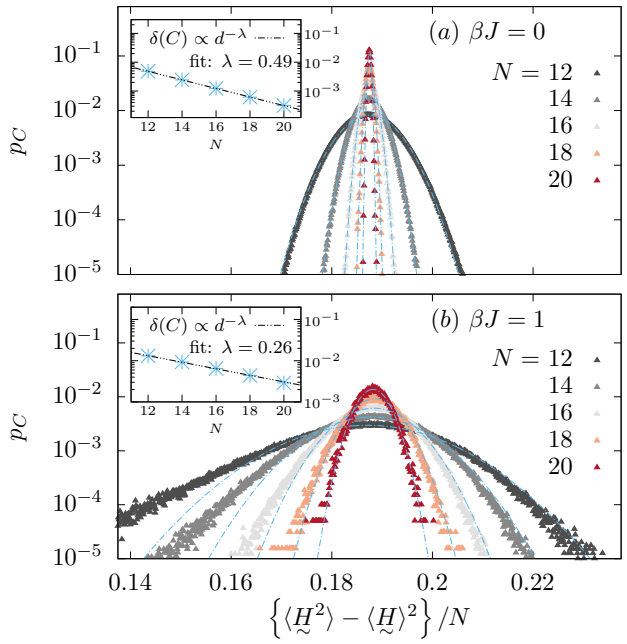


Figure 3. Analogous data as in Fig. 1, but now for the heat capacity $C(T)T^2/N$.

that although p_χ becomes narrower for larger N also at $\beta J = 1$, this scaling is now considerably slower as a function of dimension d (see inset of Fig. 1 (b)). This is caused by the smaller effective Hilbert-space dimension $Z_{\text{eff}} < d$ at $\beta J > 0$. As a consequence, for a fixed value of N, the single-state estimate in Eq. (1) becomes less reliable at $\beta J = 1$ compared to $\beta J = 0$. However, let us stress that accurate calculations are still possible at $T > 0$ as long as N is sufficiently large. (Recall, that $N \leq 20$ was chosen to be able to generate a large set of random vectors.)

In order to analyze the development of the probability distribution with respect to temperature in more detail, Fig. 2 (a) shows p_χ for various values of βJ in the range $0 \leq \beta J \leq 2$, for a fixed small system size $N = 12$. Note that the qualitative behavior in principle is independent of N, but better to visualize for small N with a broader p_χ. Starting from the high-temperature limit $\lim_{T\to\infty} \chi(T)T/N = 1/4$, we find that the maximum of p_χ gradually shifts towards smaller values upon decreasing T.

This shift of the maximum is clearly visualized also in Fig. 2 (b), which shows the same data, but in a different style. Moreover, Fig. 2 (b) additionally highlights the fact that the probability distribution p_χ for a fixed (and small) value of N becomes broader (and asymmetric) for intermediate values of T. Note, that p_χ might become narrower again for smaller values of T, see also discussion

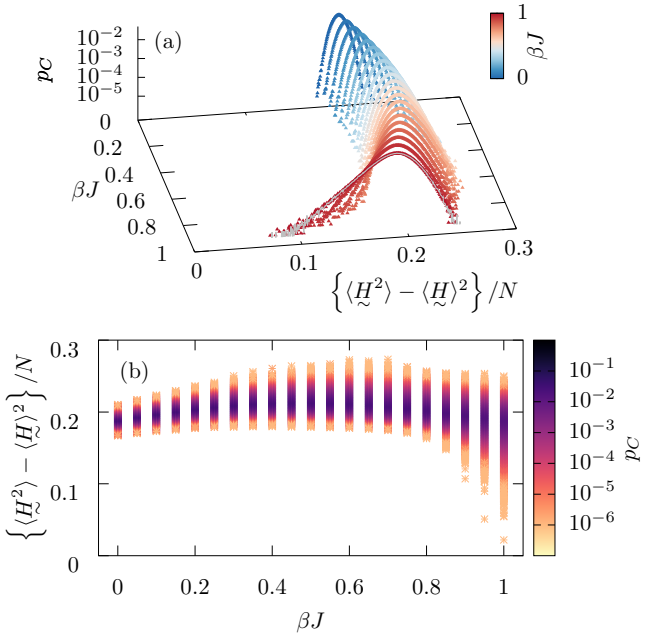


Figure 4. Analogous data as in Fig. 2, but now for the heat capacity $C(T)T^2/N$.

in Secs. III B - III C.

Eventually, in Fig. 3 and Fig. 4, we present analogous results for the full probability distribution p, but now for the heat capacity $C(T)T^2/N$. Overall, our findings for p_C are very similar compared to the previous discussion of p_χ. Namely, we find that at $\beta J = 0$, p_C is very well

described by Gaussians over several orders of magnitude. Moreover, the standard deviation $\delta(C)$ again scales as $\propto 1/\sqrt{d}$ at $\beta = 0$. As shown in Fig. 3 (b) and also in Fig. 4, the emerging asymmetry of the probability distribution at small N and finite T is found to be even more pronounced for the heat capacity compared to the previous results for $\chi(T)$. Interestingly, we find that the maximum of p_C, on the contrary, displays only a minor dependence on temperature (at least for the values of βJ shown in Fig. 4 - naturally, it is expected to change at lower temperatures and will to go to zero at temperature $T = 0$).

B. Larger antiferromagnetic spin-1/2 chains

Using a Krylov-space expansion one can nowadays reach large system sizes of $N \in [40, 50]$ for spins $s = 1/2$, see e.g. [35]. But since we also perform a statistical analysis we restrict calculations to $N \leq 36$ spins.

Following the scaling behavior of $\{\langle(\underset{\sim}{S}^z)^2\rangle - \langle\underset{\sim}{S}^z\rangle^2\}$ as well as $\{\langle\underset{\sim}{H}^2\rangle - \langle\underset{\sim}{H}\rangle^2\}$, which is shown in Figs. 1 and 3, one expects a very narrow distribution of both quantities for $N = 36$ compared to e.g. $N = 20$ since the dimension is $2^{16} = 65536$ times bigger for $N = 36$ which yields a 256 times narrower distribution. Such a distribution is smaller than the linewidth in a plot.

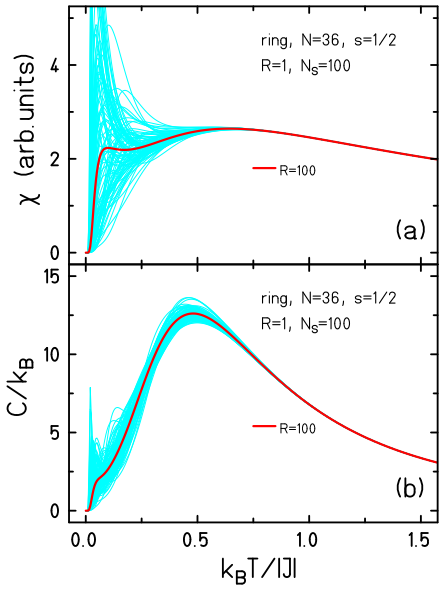


Figure 5. Spin ring $N = 36$, $s = 1/2$: The light-blue curves depict 100 different estimates of the susceptibility (a) as well as of the heat capacity (b). The FTLM estimate for $R = 100$ is also presented.

That the distributions are narrow can be clearly seen by eye inspection in Fig. 5 where the light blue curves depict thermal expectation values according to Eq. (1). For $k_BT > |J|$ they fall on top of each other and coincide

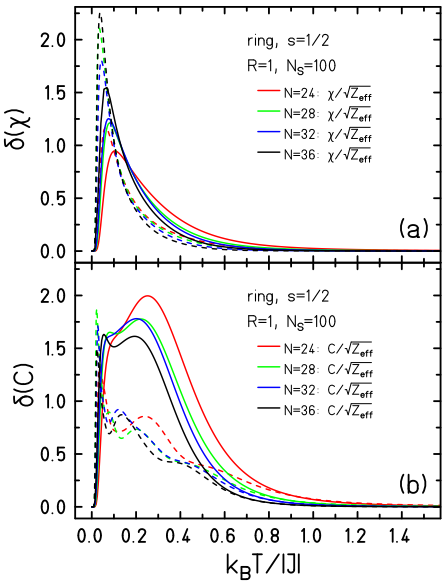


Figure 6. Spin rings, $s = 1/2$: Computed standard deviations (dashed curves) of the susceptibility (a) and the heat capacity (b) compared to the error estimate (solid curves) for various sizes N. The same color denotes the same system.

with the average over $R = 100$ realizations. Below this temperature the distributions widen, which is magnified by the fact that the real physical quantities susceptibility and heat capacity contain factors of $1/T$ and $1/T^2$, respectively.

Their standard deviation is provided in Fig. 6. Coming from high temperatures, the universal behavior (8) switches to a behavior that in general depends on system (here chain) and size below a characteristic temperature, here $k_BT \approx |J|$. Nevertheless, the qualitative expectation that the standard deviation shrinks with increasing system size is met down to $k_BT \approx 0.2|J|$, below which no definite statement about the dependence on system size can be made. We conjecture that with growing N the increasing density of low-lying states as well as the vanishing excitation gap between singlet ground state and triplet first excited state influence the behavior at very low temperatures strongly.

C. Antiferromagnetic spin-1 chains

In order to monitor an example where a vanishing excitation gap cannot be expected, not even in the thermodynamic limit, we study spin-1 chains that show a Haldane gap [36, 37], see Fig. 7. The scaling formula (8) indeed suggests that for $k_BT \lesssim (0.4 \ldots 0.5)|J|$ the standard deviations of the larger system with $N = 24$ should exceed those of the smaller system with $N = 20$, compare crossing curves of the estimator in Fig. 8. However, the actual simulations show that this is not the case. The low-temperature fluctuations in the gap region are

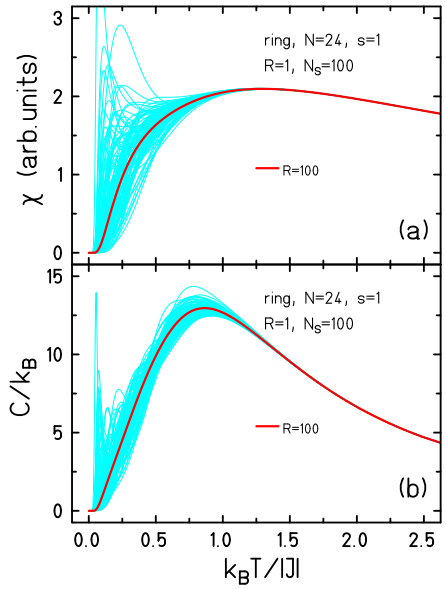


Figure 7. Spin ring $N = 24$, $s = 1$: The light-blue curves depict 100 different estimates of the susceptibility (a) as well as the heat capacity (b). The FTLM estimate for $R = 100$ is also presented.

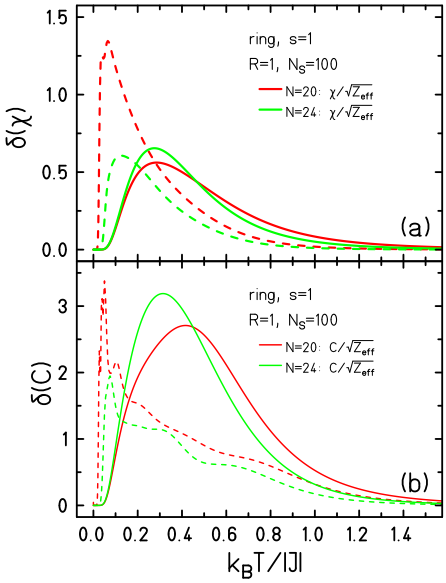


Figure 8. Spin rings, $s = 1$: Computed standard deviations (dashed curves) of the susceptibility (a) and the heat capacity (b) compared to the error estimate (solid curves) for various sizes N. The same color denotes the same system.

smaller for the larger system, at least for the two investigated system sizes.

D. Critical Spin-1/2 delta chains

As the final one-dimensional example we investigate a delta chain (also called sawtooth chain) in the quantum critical region, i.e., thermally excited above the quantum critical point (QCP) [38–40]. The QCP is met when the ferromagnetic nearest-neighbor interaction J_1 and the antiferromagnetic next-nearest neighbor interaction J_2 between spins on adjacent odd sites assume a ratio of $|J_2/J_1| = 1/2$. At the QCP the system features a massive ground-state degeneracy due to multimagnon flat bands as well as a double-peak density of states [21, 38, 39]. Moreover, the typical finite-size gap is virtually not present at the QCP [38].

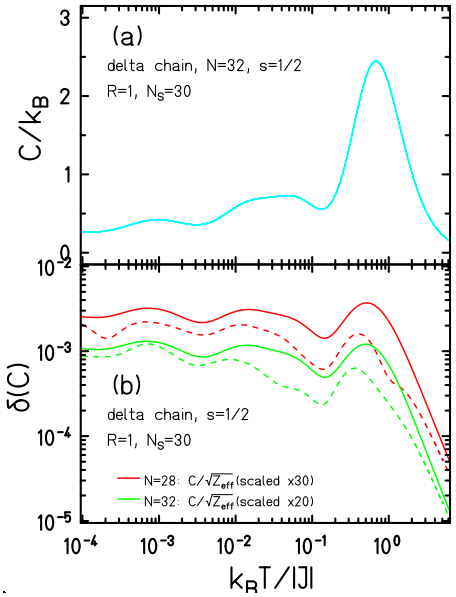


Figure 9. Delta chain $s = 1/2$, $|J_2/J_1| = 0.5$: heat capacity for $N = 32$ (a) and standard deviation for $N = 28$ and $N = 32$ (b). The light-blue curves depict $N_S = 30$ different estimates of the heat capacity (there are indeed 30 curves in this plot, which are indistinguishable by eye). Computed standard deviations (dashed curves) are compared to the error estimate (solid curves). The same color denotes the same system.

Since the QCP does not depend on the size of the system and the structure of the analytically known multimagnon flat band energy eigenstates does not either, we do not expect to find large finite-size effects when investigating the standard deviation of observables, e.g. of the heat capacity. It turns even out that by eye inspection no fluctuations are visible in Fig. 9 (a). The figure shows $N_S = 30$ thermal expectation values (3) that virtually fall on top of each other. This means that a single random vector provides the equilibrium thermodynamic functions for virtually all temperatures. When evaluating the standard deviation, dashed curves in Fig. 9 (b), it turns out that it is unusually small, even for very low temperatures. The estimator (8) to which we compare had to be scaled in this case which might have two rea-

sons. One reason could be that the large ground state degeneracy cannot be fully captured by the Krylov space expansion and thus the evaluation of the estimator (8) by means of Eq. (4) is inaccurate. The other reason could be that the empirical finding of $\alpha \approx 1$ is not appropriate in this special case of a quantum critical system. However, the general rule that trace estimators are more accurate in larger Hilbert spaces is also observed here. The standard deviation of the smaller delta chain with $N = 28$ is a few times larger than for $N = 32$.

The result is an impressive example for what it means that a quantum critical system does not possess any intrinsic scale in the quantum critical region [41, 42]. The only available scale is temperature. This means in particular that the low-energy spectrum is dense and therefore does not lead to any visible fluctuations of the estimated observables.

E. Antiferromagnetic cuboctahedra with spins 3/2, 2, and 5/2

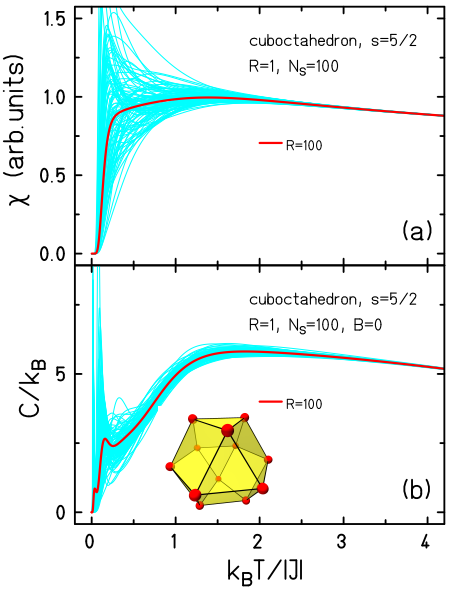


Figure 10. Cuboctahedron $N = 12$, $s = 5/2$: The light-blue curves depict 100 different estimates of the susceptibility (a) as well as the heat capacity (b). The FTLM estimate for $R = 100$ is also presented. The structure of the cuboctahedron is displayed in (b).

Our last scaling analysis differs from the previous examples. The cuboctahedron is a finite-size body, that is equivalent to a kagome lattice with $N = 12$ [43–45]. The structure is shown in Fig. 10(b). Here, we vary the spin quantum number, not the size of the system. The dimension of the respective Hilbert spaces grows considerably which leads to the expected scaling (8) above temperatures of $k_BT \approx 1.5|J|$. But the low-temperature behavior, in particular of the heat capacity for temperatures below the crossing of the estimators, eludes the expected order of more accurate results, i.e. smaller fluctuations for larger Hilbert-space dimension.

While the low-temperature behavior and the standard deviation of the susceptibility are largely governed by the energy gap between singlet ground state and triplet excited state, and this does not vary massively with the spin quantum number, the heat capacity is subject to stronger changes. When going from smaller to larger spin quantum numbers the strongly frustrated spin system looses some of its characteristic quantum properties while becoming more classical with increasing spin s. In particular, the low-lying singlet states below the first triplet state which dominate the low-temperature heat capacity move out of the gap for larger spin s [46, 47].

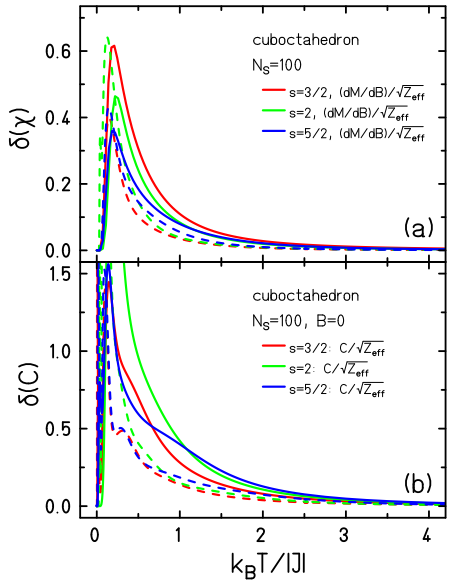


Figure 11. Cuboctahedron $N = 12$: Computed standard deviations (dashed curves) of the susceptibility (a) and the heat capacity (b) compared to the error estimate (solid curves) for various spin quantum numbers s. The same color denotes the same system.

It may thus well be that the type of Hilbert space enlargement, due to growing system size which leads to the thermodynamic limit or growing spin quantum number which leads to the classical limit, is important for the behavior of the estimators (1) and (2) at low temperatures.

IV. DISCUSSION AND CONCLUSIONS

To summarize, we have studied the finite-size scaling of typicality-based trace estimators. In these approaches, the trace over the high-dimensional Hilbert space is approximated by either (i) a single random state $|r\rangle$ or (ii) the average over a set ($R \ll d$) of random vectors. In particular, we have focused on the evaluation of thermodynamic observables such as the heat capacity and the

magnetic susceptibility for various spin models of Heisenberg type. Here, the temperature dependence of these quantities has been generated by means of a Krylov-space expansion where the random states $|r\rangle$ are used as a starting vector for the expansion.

As a first step, we have studied the full probability distribution of expectation values evaluated with respect to single random states. As an important result, we have demonstrated that for sufficiently high temperatures and large enough system sizes (i.e. sufficiently large effective Hilbert-space dimension $Z_{\rm eff}$), the probability distributions are very well described by Gaussians [33]. In particular, for comparatively high temperatures, our numerical analysis has confirmed that the standard deviation of the probability distribution scales as $\delta(O) \propto 1/\sqrt{Z_{\rm eff}}$, and that this width already describes the full distribution.

In contrast, for lower temperatures, we have shown that (i) the probability distributions can become non-Gaussian and (ii) the scaling of $\delta(O)$ can become more complicated and generally depends on the specific model and observable under consideration. While a larger Hilbert-space dimension often leads to an improved accuracy of the random-state approach at low temperatures as well, compare the investigation on kagome lattice antiferromagnets of sizes $N = 30$ and $N = 42$ in [35], we have also provided examples where this expectation can break down for too small $Z_{\rm eff}$, compare also [48].

A remarkable example is provided by the spin-1/2 sawtooth chain with coupling-ratio $|J_2/J_1| = 1/2$. Due to the (virtually) gapless dense low-energy spectrum at the quantum critical point, we have found that statistical fluctuations remain negligible throughout the entire temperature range with only minor dependence on system size (see also Ref. [49] for a similar finding in a spin-liquid model).

In conclusion, we have demonstrated that typicality-based estimators provide a convenient numerical tool in order to accurately approximate thermodynamic observables for a wide range of temperatures and models. While in some cases, even a single pure state is sufficient, the accuracy of the results can always be improved by averaging over a set of independently drawn states.

ACKNOWLEDGMENT

This work was supported by the Deutsche Forschungsgemeinschaft DFG (397067869 (STE 2243/3-1); 355031190 (FOR 2692); 397300368 (SCHN 615/25-1)). Computing time at the Leibniz Center in Garching is gratefully acknowledged. All authors thank Hans De Raedt, Peter Prelovšek, Patrick Vorndamme, Peter Reimann, Jochen Gemmer as well as Katsuhiro Morita for valuable comments.

[1] J. Jaklič and P. Prelovšek, "Lanczos method for the calculation of finite-temperature quantities in correlated systems," Phys. Rev. B **49**, 5065 (1994).
[2] J. Jaklič and P. Prelovšek, "Finite-temperature properties of doped antiferromagnets," Adv. Phys. **49**, 1 (2000).
[3] I. Zerec, B. Schmidt, and P. Thalmeier, "Kondo lattice model studied with the finite temperature Lanczos method," Phys. Rev. B **73**, 245108 (2006).
[4] J. Schnack and O. Wendland, "Properties of highly frustrated magnetic molecules studied by the finite-temperature Lanczos method," Eur. Phys. J. B **78**, 535 (2010).
[5] O. Hanebaum and J. Schnack, "Advanced finite-temperature Lanczos method for anisotropic spin systems," Eur. Phys. J. B **87**, 194 (2014).
[6] E. Pavarini, E. Koch, R. Scalettar, and R. M. Martin, eds., "The Physics of Correlated Insulators, Metals, and Superconductors," (2017) Chap. The Finite Temperature Lanczos Method and its Applications by P. Prelovšek, ISBN 978-3-95806-224-5, http://hdl.handle.net/2128/15283.
[7] B. Schmidt and P. Thalmeier, "Frustrated two dimensional quantum magnets," Phys. Rep. **703**, 1 (2017).
[8] J. Skilling, "Maximum Entropy and Bayesian Methods," (Kluwer, Dordrecht, 1988) Chap. The eigenvalues of mega-dimensional matrices, pp. 455–466.
[9] M. Hutchinson, "A Stochastic Estimator of the Trace of the Influence Matrix for Laplacian Smoothing Splines," Communications in Statistics - Simulation and Computation **18**, 1059 (1989).
[10] D. A. Drabold and O. F. Sankey, "Maximum entropy approach for linear scaling in the electronic structure problem," Phys. Rev. Lett. **70**, 3631 (1993).
[11] R. N. Silver and H. Röder, "Densities of states of mega-dimensional Hamiltonian matrices," Int. J. Mod. Phys. C **5**, 735 (1994).
[12] G. H. Golub and U. von Matt, *Tikhonov Regularization for Large Scale Problems*, Tech. Rep. (Stanford University, 1997) technical report SCCM-97-03.
[13] A. Weiße, G. Wellein, A. Alvermann, and H. Fehske, "The kernel polynomial method," Rev. Mod. Phys. **78**, 275 (2006).
[14] H. Avron and S. Toledo, "Randomized Algorithms for Estimating the Trace of an Implicit Symmetric Positive Semi-definite Matrix," J. ACM **58**, 8:1 (2011).
[15] F. Roosta-Khorasani and U. Ascher, "Improved Bounds on Sample Size for Implicit Matrix Trace Estimators," Found. Comput. Math. **15**, 1187 (2015).
[16] A. K. Saibaba, A. Alexanderian, and I. C. F. Ipsen, "Randomized matrix-free trace and log-determinant estimators," Numer. Math. **137**, 353 (2017).
[17] K. Inoue, Y. Maeda, H. Nakano, and Y. Fukumoto, "Canonical-Ensemble Calculations of the Magnetic Susceptibility for a Spin-1/2 Spherical Kagome Cluster with Dzyaloshinskii-Moriya Interactions by Using Microcanonical Thermal Pure Quantum States," IEEE Transactions on Magnetics **55**, 1 (2019).

[18] S. Sugiura and A. Shimizu, "Thermal Pure Quantum States at Finite Temperature," Phys. Rev. Lett. **108**, 240401 (2012).

[19] S. Sugiura and A. Shimizu, "Canonical Thermal Pure Quantum State," Phys. Rev. Lett. **111**, 010401 (2013).

[20] S. Okamoto, G. Alvarez, E. Dagotto, and T. Tohyama, "Accuracy of the microcanonical Lanczos method to compute real-frequency dynamical spectral functions of quantum models at finite temperatures," Phys. Rev. E **97**, 043308 (2018).

[21] J. Schnack, J. Richter, and R. Steinigeweg, "Accuracy of the finite-temperature Lanczos method compared to simple typicality-based estimates," Phys. Rev. Research (2020), in print, arXiv:1911.08838 [cond-mat.str-el].

[22] B. Collins and P. Śniady, "Integration with Respect to the Haar Measure on Unitary, Orthogonal and Symplectic Group," Commun. Math. Phys. **264**, 773 (2006).

[23] C. Bartsch and J. Gemmer, "Dynamical Typicality of Quantum Expectation Values," Phys. Rev. Lett. **102**, 110403 (2009).

[24] P. Reimann, "Typical fast thermalization processes in closed many-body systems," Nature Communications **7**, 10821 (2016).

[25] H. Tal-Ezer and R. Kosloff, "An accurate and efficient scheme for propagating the time dependent Schrödinger equation," J. Chem. Phys. **81**, 3967 (1984).

[26] V. V. Dobrovitski and H. De Raedt, "Efficient scheme for numerical simulations of the spin-bath decoherence," Phys. Rev. E **67**, 056702 (2003).

[27] R. Steinigeweg, J. Gemmer, and W. Brenig, "Spin-current autocorrelations from single pure-state propagation," Phys. Rev. Lett. **112**, 120601 (2014).

[28] R. Steinigeweg, J. Gemmer, and W. Brenig, "Spin and energy currents in integrable and nonintegrable spin-$\frac{1}{2}$ chains: A typicality approach to real-time autocorrelations," Phys. Rev. B **91**, 104404 (2015).

[29] T. A. Elsayed and B. V. Fine, "Regression Relation for Pure Quantum States and Its Implications for Efficient Computing," Phys. Rev. Lett. **110**, 070404 (2013).

[30] J. Schulenburg, *spinpack 2.56*, Magdeburg University (2017).

[31] J. Richter and J. Schulenburg, "The spin-1/2 J_1-J_2 Heisenberg antiferromagnet on the square lattice: Exact diagonalization for N=40 spins," Eur. Phys. J. B **73**, 117 (2010).

[32] A. Hams and H. De Raedt, "Fast algorithm for finding the eigenvalue distribution of very large matrices," Phys. Rev. E **62**, 4365 (2000).

[33] P. Reimann and J. Gemmer, "Full expectation-value statistics for randomly sampled pure states in high-dimensional quantum systems," Phys. Rev. E **99**, 012126 (2019), arXiv:1901.05784.

[34] H.-J. Schmidt, J. Schnack, and M. Luban, "Heisenberg exchange parameters of molecular magnets from the high-temperature susceptibility expansion," Phys. Rev. B **64**, 224415 (2001).

[35] J. Schnack, J. Schulenburg, and J. Richter, "Magnetism of the $N = 42$ kagome lattice antiferromagnet," Phys. Rev. B **98**, 094423 (2018).

[36] F. D. M. Haldane, "Continuum dynamics of the 1-d Heisenberg anti-ferromagnet - identification with the o(3) non-linear sigma-model," Phys. Lett. A **93**, 464 (1983).

[37] F. D. M. Haldane, "Non-linear field-theory of large-spin Heisenberg antiferromagnets - semi-classically quantized solitons of the onedimensional easy-axis neel state," Phys. Rev. Lett. **50**, 1153 (1983).

[38] V. Y. Krivnov, D. V. Dmitriev, S. Nishimoto, S.-L. Drechsler, and J. Richter, "Delta chain with ferromagnetic and antiferromagnetic interactions at the critical point," Phys. Rev. B **90**, 014441 (2014).

[39] D. V. Dmitriev and V. Y. Krivnov, "Delta chain with anisotropic ferromagnetic and antiferromagnetic interactions," Phys. Rev. B **92**, 184422 (2015).

[40] A. Baniodeh, N. Magnani, Y. Lan, G. Buth, C. E. Anson, J. Richter, M. Affronte, J. Schnack, and A. K. Powell, "High spin cycles: topping the spin record for a single molecule verging on quantum criticality," npj Quantum Materials **3**, 10 (2018).

[41] T. Vojta, "Quantum phase transitions in electronic systems," Ann. Phys. **9**, 403 (2000).

[42] M. Vojta, "Quantum phase transitions," Rep. Prog. Phys. **66**, 2069 (2003).

[43] I. Rousochatzakis, A. M. Läuchli, and F. Mila, "Highly frustrated magnetic clusters: The kagomé on a sphere," Phys. Rev. B **77**, 094420 (2008).

[44] A. Honecker and M. E. Zhitomirsky, "Magneto-thermal properties of the spin-s Heisenberg antiferromagnet on the cuboctahedron," J. Phys.: Conf. Ser. **145**, 012082 (4pp) (2009).

[45] H.-J. Schmidt, A. Hauser, A. Lohmann, and J. Richter, "Interpolation between low and high temperatures of the specific heat for spin systems," Phys. Rev. E **95**, 042110 (2017).

[46] R. Schmidt, J. Schnack, and J. Richter, "Frustration effects in magnetic molecules," J. Magn. Magn. Mater. **295**, 164 (2005).

[47] J. Schnack and R. Schnalle, "Frustration effects in antiferromagnetic molecules: the cuboctahedron," Polyhedron **28**, 1620 (2009).

[48] K. Morita and T. Tohyama, "Finite-temperature properties of the Kitaev-Heisenberg models on kagome and triangular lattices studied by improved finite-temperature Lanczos methods," ArXiv e-prints (2019), arXiv:1911.09266 [cond-mat.str-el].

[49] I. Rousochatzakis, S. Kourtis, J. Knolle, R. Moessner, and N. B. Perkins, "Quantum spin liquid at finite temperature: Proximate dynamics and persistent typicality," Phys. Rev. B **100**, 045117 (2019).